Available online at www.sciencedirect.com

SCIENCE DIRECT®

Earth and Planetary Science Letters 224 (2004) 55–72

EPSL

www.elsevier.com/locate/epsl

Detection, quantification, and significance of hiatuses in pelagic and hemipelagic strata

Stephen R. Meyers[a,*], Bradley B. Sageman[b,1]

[a] Department of Geology and Geophysics, Yale University, P.O. Box 208109, New Haven, CT 06520-8190, USA
[b] Department of Geological Sciences, Northwestern University, Evanston, IL 60208, USA

Received 26 January 2004; received in revised form 30 April 2004; accepted 4 May 2004

Abstract

Temporal gaps in the stratigraphic record have important implications for the interpretation of stratigraphically rapid geochemical and paleobiologic changes, for the development of high-resolution time scales (e.g., orbital time scales), and for deciphering the response of depositional systems to climatic change and basin evolution (e.g., accommodation space vs. sediment supply). In ancient pelagic and hemipelagic strata, the identification of relatively short hiatus (10^3–10^6 years) is commonly challenged by the resolution limits of geochronologic techniques. In this study, a quantitative method is developed to identify and quantify hiatuses in strata where Milankovitch orbital cycles are documented. The new method is based on the interpretation of evolutive harmonic analysis (EHA) results and permits estimation of minimum durations for the temporal gaps. Application of this technique to an optical densitometry data series derived from the Cenomanian/Turonian (C/T) Bridge Creek Limestone Member permits quantification of hiatus within the unit and addresses important questions about abrupt changes in biogeochemical proxy records across the boundary interval. Integration of the new method with stratigraphic data and geochemical burial flux estimates permits a detailed reconstruction of the controls on sediment delivery and hiatus generation, including a refined analysis of the orbital-scale linkages between climate and sedimentation.

Keywords: EHA; hiatus; C/T; OAE II; Milankovitch

1. Introduction

Sedimentary bedding rhythms have been employed for the analysis of time–rock relationships by a number of investigators [1–5]. In addition to improving the accuracy of geologic time scales, the ability to construct a high-resolution orbital chronology for a study interval significantly enhances the power and scope of sedimentologic, paleobiologic, and geochemical investigations. Such time scales permit detailed calculation of rates of accumulation for biogeochemical proxies [6] and also allow rates of change in paleobiologic or sedimentologic parameters to be determined [7].

The multi-component (precession, obliquity, and eccentricity) nature of orbital forcing makes its expression sensitive to stratigraphic hiatus over a broad range of time scales, but such temporal gaps have historically been treated as a source of error in the development of orbital chronologies. Previous efforts to identify and quantify hiatus in hemipelagic and pelagic strata have

* Corresponding author. Tel.: +1-203-432-8343; fax: +1-203-432-3134.
E-mail addresses: stephen.meyers@yale.edu (S.R. Meyers), brad@earth.northwestern.edu (B.B. Sageman).
[1] Tel.: +1-847-467-2257; fax: +1-847-491-8060.

0012-821X/$ - see front matter © 2004 Elsevier B.V. All rights reserved.
doi:10.1016/j.epsl.2004.05.003

largely relied upon biostratigraphy [8–13], which depends on the availability of reliable biostratigraphic datums and the development of composite standards, and has inherent resolution limits that define the shortest resolvable hiatus. House [14] suggested that the maximum zonal resolution achievable using biozonation schemes may be as low as 500 kyr, although claims for finer resolution have been made in special cases (e.g., composite assemblage zones of Kauffman et al. [15]).

Previous studies [6,16] have demonstrated that hiatus in cyclostratigraphic records results in frequency domain (e.g., power spectum) distortion. In this paper, a new technique for the identification and quantification of hiatus using spectral analysis of rhythmically bedded strata is presented. This technique exploits the fact that orbital cycles (e.g., precession, obliquity, eccentricity) provide multiple stratigraphically imbedded time scales, each of which may be distorted by hiatus. Using stratigraphic modeling, Meyers et al. [6] initially demonstrated that hiatus in rhythmic strata may be detected via evolutive harmonic analysis (EHA; a moving window Fourier analysis that employs the multi-taper method (MTM) of Thomson [17] to identify significant harmonic components) of stratigraphic data series. Here, the EHA methodology for hiatus detection and quantification is fully developed and applied, including discussion of the theory underlying this technique, a discussion of its resolution limitations, and an example of its application.

Signal distortion representing hiatus was first detected during our initial applications of the EHA method to the Bridge Creek Limestone Member of the Greenhorn Formation, a rhythmically bedded hemipelagic unit deposited during Cenomanian/Turonian (C/T) time in the Western Interior sea [6]. Because this stratigraphic interval contains significant and abrupt shifts in geochemical parameters [18,19] associated with a hypothesized oceanic anoxic event (OAE II: Schlanger et al. [20]), as well as the stepwise molluscan extinction horizons of the C/T boundary [21,22], the recognition of stratigraphic gaps in this interval is particularly important. When geologic observations provided evidence for the presence of hiatus at the level of EHA signal distortion, a method to scale the distortion to time lost from the stratigraphic time series was investigated and developed. This study employs a high-resolution optical densitometry data set, independent time control from $^{40}Ar–^{39}Ar$ dates intercalated within the studied section [23,24] and a robust set of complimentary stratigraphic, sedimentologic, and paleobiologic observations. As such, the Bridge Creek Limestone Member provides an excellent case study for development of this new method.

2. Methods

2.1. The EHA-$\Delta\mu$ method

In noisy stratigraphic records of orbital forcing, and cyclic units that preserve multiple orbital components (which may vary in their dominance through time (e.g., de Menocal [25]), obvious stratigraphic expressions of hiatus, such as disruption of the $\sim$5:1 precession–eccentricity syndrome, may be masked by complex bedding patterns such as those reflecting the combined influence of multiple orbital signals. However, such discontinuities may be clearly identified in the frequency domain via evolutive harmonic analysis. The presence of hiatus in stratigraphic records of orbital forcing results in a distinctive frequency domain expression: an amplitude (μ) response characterized by bifurcation of the primary frequency component into two smaller side lobes. Fig. 1 demonstrates this phenomena with a simple monochromatic signal, through analysis of a 2-m-long record of a synthetic stratigraphic parameter (sampled every 1 cm) generated to express a 40-kyr periodicity, with a background sedimentation rate of 0.5 cm/kyr, and a 20-kyr hiatus at 1 m. The hiatus results in bifurcation of the original primary frequency (5 cycles/m) into two new frequencies (4.5 and 5.5 cycles/m).

Characterization of the relationship between hiatus duration and its frequency domain amplitude bifurcation is displayed in Fig. 2. This analysis reveals that the amplitudes of the bifurcated peaks of the signal provide a means to reconstruct the amount of time missing due to hiatus. In Fig. 2, the amplitude difference ($\Delta\mu$) between bifurcated peaks is plotted against fractional hiatus duration (the fraction of the periodicity removed in each model data point in Fig. 2). The amplitude difference is defined as

$$\Delta\mu = \frac{\mu_1 - \mu_2}{\mu_1 + \mu_2}$$

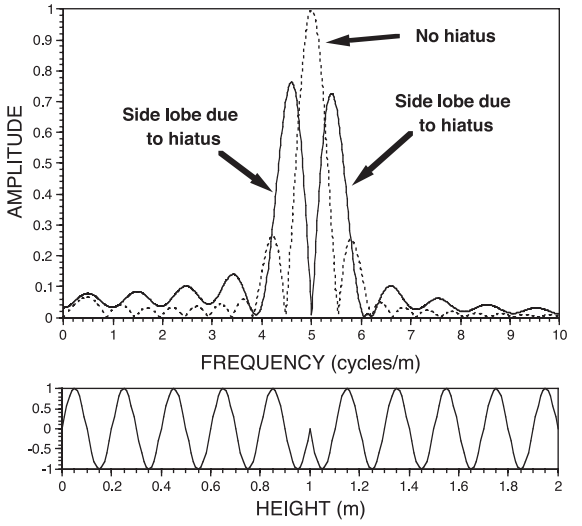

Fig. 1. Harmonic analysis of a synthetic stratigraphic parameter generated to express a 40-kyr periodicity, with a background sedimentation rate of 0.5 cm/kyr, and a 20-kyr hiatus at 1 m. The lower plot displays the synthetic stratigraphic data series and the upper plot displays its amplitude spectrum. The hiatus at 1 m results in bifurcation of the original primary frequency (5 cycles/m) into two new frequencies (4.5 and 5.5 cycles/m). The dashed line in the amplitude spectrum represents the same synthetic stratigraphic data series without hiatus.

where μ_1 is the amplitude of the lower-frequency component and μ_2 is the amplitude of the higher-frequency component. The calculation of $\Delta\mu$ includes normalization to the sum of the amplitudes of the bifurcated peaks, which facilitates the application of this relationship to a variety of cyclostratigraphic records. Fig. 2 demonstrates that the frequency domain $\Delta\mu$ value has a linear relationship to hiatus duration in these models of monochromatic sinusoids.

Application of the EHA-$\Delta\mu$ technique to reconstruct hiatus duration is depicted in Fig. 3. In this example, a 6-m-long synthetic model has been generated to express a 40-kyr periodicity (background sedimentation rate of 0.5 cm/kyr) with a 10-kyr hiatus at a height of 3 m (Fig. 3A). Evolutive harmonic analysis of this model (using a 2-m window) demonstrates the distinctive signature of hiatus (Fig. 3B): (1) as the 2-m window approaches the hiatus location, the primary signal (5 cycles/m) is bifurcated into two new components, and (2) once the 2-m window passes the hiatus location the bifurcated components amalgamate back into the original signal of 5 cycles/m. This characteristic amplitude distortion differs from the spectral expression of other stratigraphic perturbations, such as rapid sedimentation rate changes in the absence of hiatus [6].

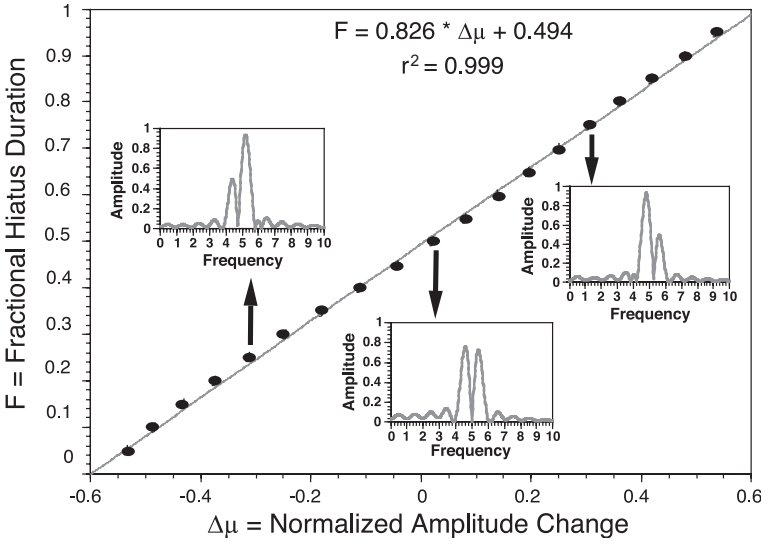

Fig. 2. Plot of normalized amplitude change ($\Delta\mu$) vs. fractional hiatus duration (F), as determined by stratigraphic modeling experiments. The inset figures show examples of amplitude spectra used to generate the data points.

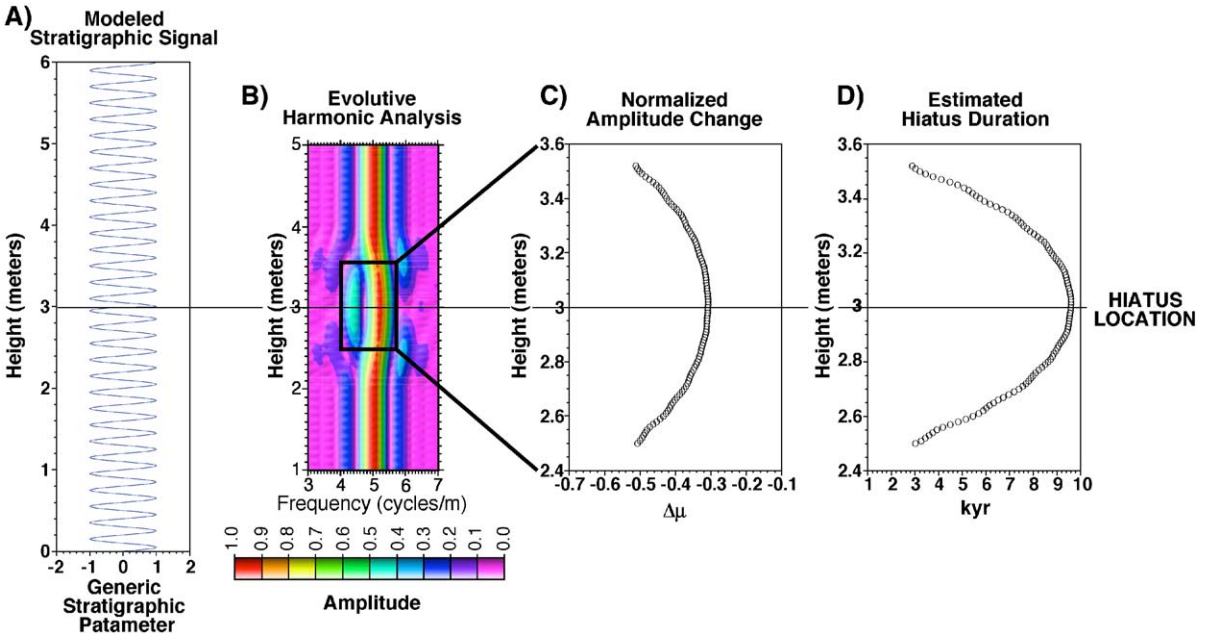

Fig. 3. Application of the EHA-$\Delta\mu$ technique to reconstruct hiatus duration. The synthetic model shown in (A) was generated to express a 40-kyr periodicity, a sedimentation rate of 0.5 cm/kyr, and a hiatus of 10 kyr at 3 m. EHA is applied to this stratigraphic model using a 2-m moving window and $3-2\pi$ tapers (B). The $\Delta\mu$ values across the interval of bifurcation are shown in (C), and the reconstructed hiatus duration is shown in (D).

In Fig. 3C, $\Delta\mu$ is calculated across the interval of bifurcation. The response of $\Delta\mu$ across this interval (which we will refer to as a "$\Delta\mu$ plot") is such that the $\Delta\mu$ value is maximized at the location of the hiatus. More generally, the location of hiatus is coincident with a maximum or minimum in $\Delta\mu$: Hiatus less than approximately half of the bifurcated periodicity will result in a maximum in $\Delta\mu$, while a hiatus greater than this will result in a minimum. Fig. 4 demonstrates this characteristic $\Delta\mu$ response using five models generated to express a 40-kyr periodicity and hiatus of increasing duration at 3 m height (4, 12, 20, 28 and 36 kyr). The $\Delta\mu$ maximum or minimum should be used for reconstruction of hiatus location and duration, using the relationship identified in Fig. 2.

2.2. EHA-$\Delta\mu$ sensitivity models

The EHA-$\Delta\mu$ hiatus reconstruction for the data series in Fig. 3 identifies a hiatus duration of 9.6 kyr, which demonstrates the level of error associated with the analysis (4.0%). However, the signature of orbital cyclicity preserved in the stratigraphic record is rarely as simple as the monochromatic model shown in Fig. 3. Employment of the EHA-$\Delta\mu$ technique to identify and reconstruct hiatus duration from mea-

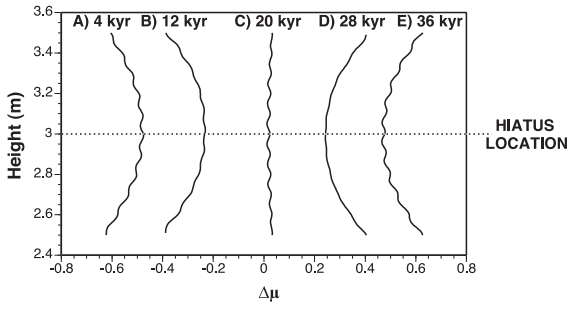

Fig. 4. EHA-$\Delta\mu$ results for five synthetic models, demonstrating the characteristic $\Delta\mu$ response for hiatus of varying duration. All models were generated to express a 40-kyr periodicity, with a sedimentation rate of 0.5 cm/kyr, and a hiatus at 3 m height. (A) 4-kyr hiatus at 3 m, (B) 12-kyr hiatus at 3 m, (C) 20-kyr hiatus at 3 m, (D) 28-kyr hiatus at 3 m, (E) 36-kyr hiatus at 3 m. For hiatus durations less than half of the 40-kyr period (A and B), the hiatus location is approximately coincident with the $\Delta\mu$ maximum. For hiatus durations greater than half of the 40-kyr period (D and E), the hiatus location is approximately coincident with the $\Delta\mu$ minimum.

sured lithologic/geochemical data is influenced by four general types of error: (1) the multi-component nature (precession, obliquity, eccentricity) of time series may complicate accurate amplitude estimation due to interference (e.g., spectral leakage) between frequency components in the spectrum, an inherent limitation of the Fast Fourier Transform (FFT) of finite data series, (2) the orbital signal is typically perturbed by some degree of background frequency noise (instability of sedimentation rate) and amplitude noise (non-orbital controls on the depositional system and analytical measurement error), (3) the ''raw'' orbital periodicity must not contain inherent bifurcations, since such frequency modulation would be incorrectly interpreted as hiatus, and (4) errors associated with temporal calibration of the spatial bedding frequencies could contribute to error in the estimated hiatus duration. The purpose of this section of the paper is to address such limitations on the EHA-$\Delta\mu$ technique via analysis of several sensitivity models.

To minimize the influence of bias in the Fast Fourier Transform of the data series (type 1 error listed above), the multi-taper method analysis of Thomson [17] is used in all modeling exercises and in the analysis of the measured stratigraphic data series. The MTM technique provides exceptional amplitude estimates in short and noisy data series. It does so by minimizing spectral leakage, through application of several statistically independent bias-resistant orthogonal data tapers. The data tapers (known as discrete

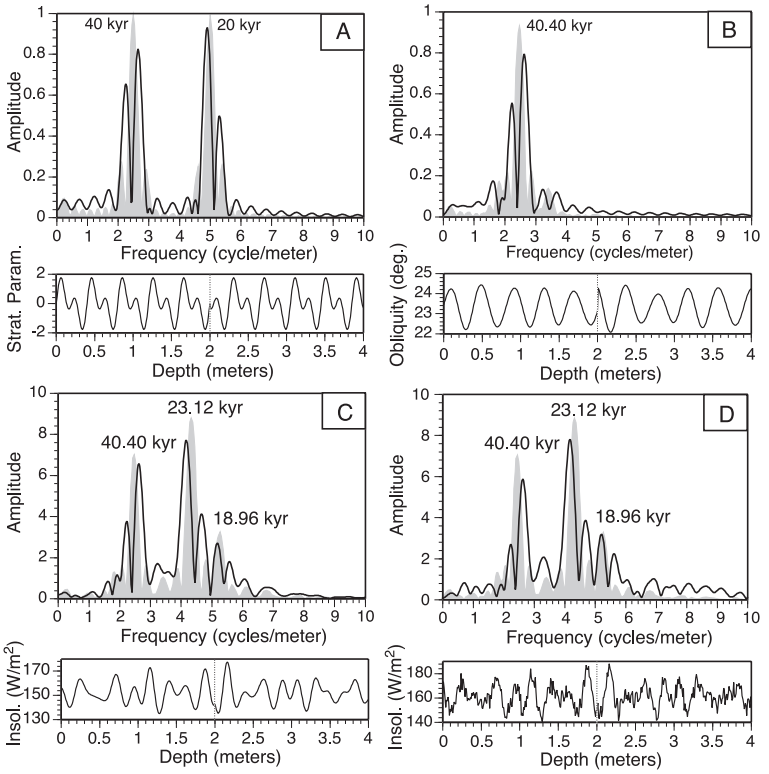

Fig. 5. Sensitivity models generated to test the reliability of the EHA-$\Delta\mu$ method. Each 4-m-long model is sampled every 1 cm, has a background sedimentation rate of 1 cm/kyr, and a 15-kyr hiatus at a depth of 2 m. (A) Model constructed from a 20-kyr (amplitude = 1, phase = 0) and 40-kyr (amplitude = 1, phase = 0) periodicity. (B) Model constructed from Laskar's [27] 0–415 kyr BP solution for obliquity. (C) Model constructed from Laskar's [27] 0–415 kyr BP solution for daily insolation at 40° North during the winter solstice. (D) Model constructed from the same insolation series as (C) with random additive amplitude noise (maximum = 25% of total variance) and random additive/subtractive frequency noise (maximum = 25% of sedimentation rate). The obliquity and insolation series [27] were calculated using the program Analyseries [28]. In all spectra, the gray-shaded spectrum displays the amplitude response when no hiatus is present and the solid line displays the amplitude response when a 15-kyr hiatus is present.

prolate spheriodal sequences or DPSSs) provide a compromise between the statistical stability of the spectral estimate and its frequency resolution, and are characterized by a "time–bandwidth" product: $n\pi$ (where n represents the duration of the time series multiplied by the desired halfwidth resolution). Fast Fourier Transforms are performed on each tapered data series, and these statistically independent results are then employed to estimate the amplitude spectrum. The MTM technique also provides a test of statistical significance (F test) for the harmonic (line) components, which is particularly useful in very noisy stratigraphic data series. See Thomson [17] and Park et al. [26] for more information on the procedure.

Fig. 5 and Table 1 display the results of four sensitivity models, each of which represents a progressively more complicated data series. Each 4-m-long model has a background sedimentation rate of 1 cm/kyr, a sampling interval of 1 cm, and a 15-kyr hiatus at a depth of 2 m. Sensitivity model A was constructed by adding a 20-kyr (amplitude = 1, phase = 0) and 40-kyr (amplitude = 1, phase = 0) periodicity. Model B was constructed from Laskar's [27] 0–415 kyr BP solution for obliquity. Model C was constructed from Laskar's [27] 0–415 kyr BP solution for daily insolation at 40° North during the winter solstice (selected because it contains large obliquity and precession amplitude contributions). Model D was constructed from the same insolation series as Model C, with random additive amplitude noise (maximum = 25% of total variance) and random additive/subtractive frequency noise (maximum = 25% of sedimentation rate).

The error associated with the $\Delta\mu$ analyses in models A and B are $\leq$7.0% (Table 1), but increase to a maximum of 27.3% for the obliquity component of the more complicated insolation series of Model C. This increase in error is due to interference (spectral leakage) between the multiple precession and obliquity terms, primarily the 40.40-, 23.12-, and 18.96-kyr components. Finally, the addition of significant amounts of frequency and amplitude noise results in errors of up to 48.7%. We propose that model D should represent a worst-case scenario for most distal hemipelagic settings, which are generally characterized by relatively slow but consistent rates of sediment accumulation on Milankovitch time scales. Therefore, when performing EHA-$\Delta\mu$ analyses on measured stratigraphic data series, we expect to estimate hiatus duration with < 50% error, and possibly as little as 6% error in data series that are dominated by an obliquity signal. Of course, given extreme amplitude and frequency noise, identification of orbital components and detection of hiatus will not be possible.

To address the third source of error outlined above (bifurcations inherent to the orbital periodicities that comprise the insolation series) we perform EHA on Laskar's [27] 0–5.5 Ma solution for daily insolation at 40° North during the winter solstice (Fig. 6). Analysis of the entire insolation series identifies 4 dominant frequency components, the 40.98-kyr obliquity term and three precession terms: 23.67, 22.38, and 18.95 kyr (amplitude spectrum at top of Fig. 6). EHA on this insolation series was conducted by employing $3-2\pi$ data tapers and a 400-kyr moving window. This analysis illuminates the inherent degree of instability of the obliquity and precessional components [29]. Most notably, the 23.67- and 22.38-kyr

Table 1
Sensitivity model results

Model	Model comments	Periodicity (kyr)	$\Delta\mu$	Estimated fraction removed	Estimated hiatus duration (kyr)	Error (%)
A	20-kyr + 40-kyr periodicity	20.00	0.302	0.743	14.9	0.7
		40.00	− 0.115	0.399	16.0	7.0
B	Obliquity (LA90), 0–415 kyr BP	40.40	− 0.177	0.348	14.1	6.0
C	Daily insolation 40°N, 270° (LA90),	18.96	0.199	0.658	12.5	16.7
	0–415 kyr BP	23.12	− 0.303	0.745	17.2	14.7
		40.40	− 0.271	0.270	10.9	27.3
D	Daily insolation 40°N, 270° (LA90),	18.96	0.175	0.639	12.1	19.3
	0–415 kyr BP, with 25% frequency +	23.12	− 0.337	0.772	17.9	19.3
	25% amplitude noise	40.40	− 0.368	0.190	7.7	48.7

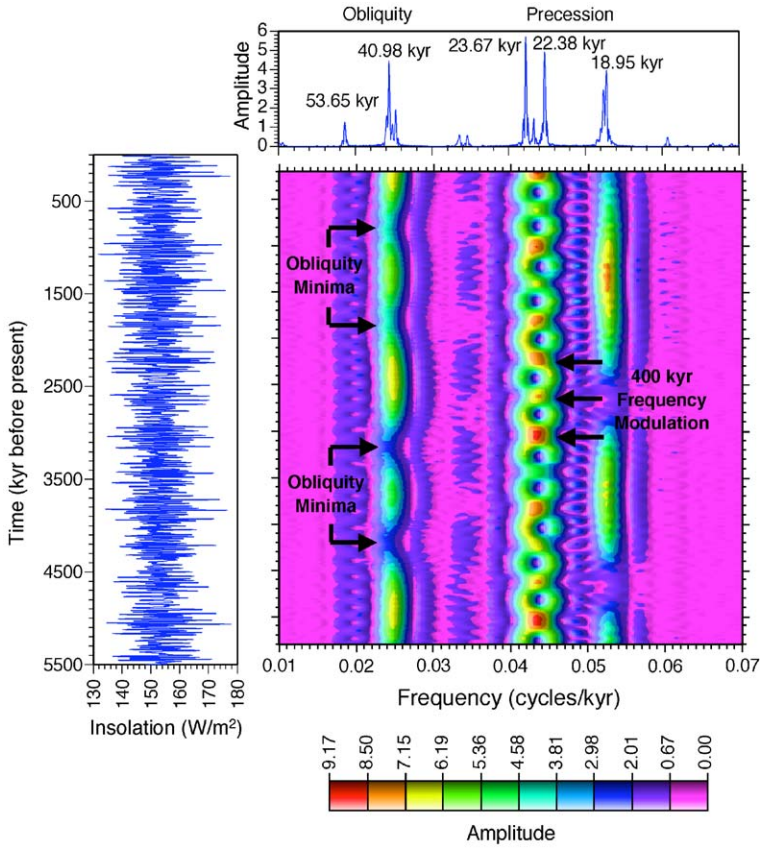

Fig. 6. EHA-$\Delta\mu$ sensitivity analysis on Laskar's [27] 0–5.5 Ma solution for daily insolation at 40° North during the winter solstice. The raw insolation data is plotted to the left of the EHA results. The amplitude spectrum for the entire data series is shown at the top of the EHA plot. The evolutive harmonic analysis employed $3-2\pi$ data tapers and a 400-kyr moving window. The insolation series [27] was calculated using the program Analyseries [28].

precessional components are characterized by a periodic signal amalgamation and bifurcation, which is linked to a 400-kyr (eccentricity) frequency modulation. A similar frequency modulation is expressed in Laskar's [27] eccentricity series, with a 400-kyr periodic bifurcation and amalgamation of the short eccentricity terms (95 and 124 kyr). Furthermore, amplitude modulation of the precession and obliquity components is clearly illustrated in Fig. 6, and may impact the EHA-$\Delta\mu$ analysis as well: during times of low signal amplitude (e.g., obliquity minima in Fig. 6), identification of hiatus-related signal bifurcations will be hindered. Based on these results, it is clear that the precession and short eccentricity terms are not optimal for EHA-$\Delta\mu$ analysis, since they contain inherent periodic bifurcations. Therefore, application of the EHA-$\Delta\mu$ method must be restricted to the dominant obliquity component (40.98 kyr) and the long eccentricity component (404 kyr). However, it is important to note that the short eccentricity and precession components will still be influenced by hiatus, although the resultant distortion will be less systematic. Furthermore, although the presence of bifurcation in the short eccentricity and precession terms is not reliable for quantification of hiatus, the absence of distortion in short eccentricity and precession components may be employed as evidence for relatively conformable deposition (lack of hiatus).

To further assess the impact of frequency and amplitude modulations on the identification and reconstruction of hiatus duration using the EHA-$\Delta\mu$ technique, the insolation data series in Fig. 6 is

employed to model 54 m of stratigraphy with 10 imbedded hiatus events of 15 kyr each (background sedimentation rate = 1 cm/kyr; sampled every 1 cm) (Fig. 7). This EHA analysis employed $3-2\pi$ tapers and a 4-m moving window. The variability in estimated hiatus duration in this sensitivity analysis ranges from 13 to 25 kyr, spanning an error range of −11% (underestimated) to 69% (overestimated). Most notably, the two hiatus events with the greatest error (hiatus 3 = 69%, hiatus 5 = 50%) are associated with the two intervals of low obliquity amplitude identified in Fig. 6. In measured stratigraphic data series, these two hiatus events would most likely go entirely unnoticed as these bifurcations are poorly expressed and barely distinguishable from the background spectrum. The next greatest level of error is associated with hiatus 9 (33%). Based on this result, we suggest that hiatus identified using the obliquity component, barring additional distortions, may be reconstructed with an error of ≤33%, and on average ≤11% error.

A final source of error in the analysis of measured stratigraphic data series concerns temporal calibration of the bifurcated spatial frequency. To address this issue, two approaches are employed. First, time con-

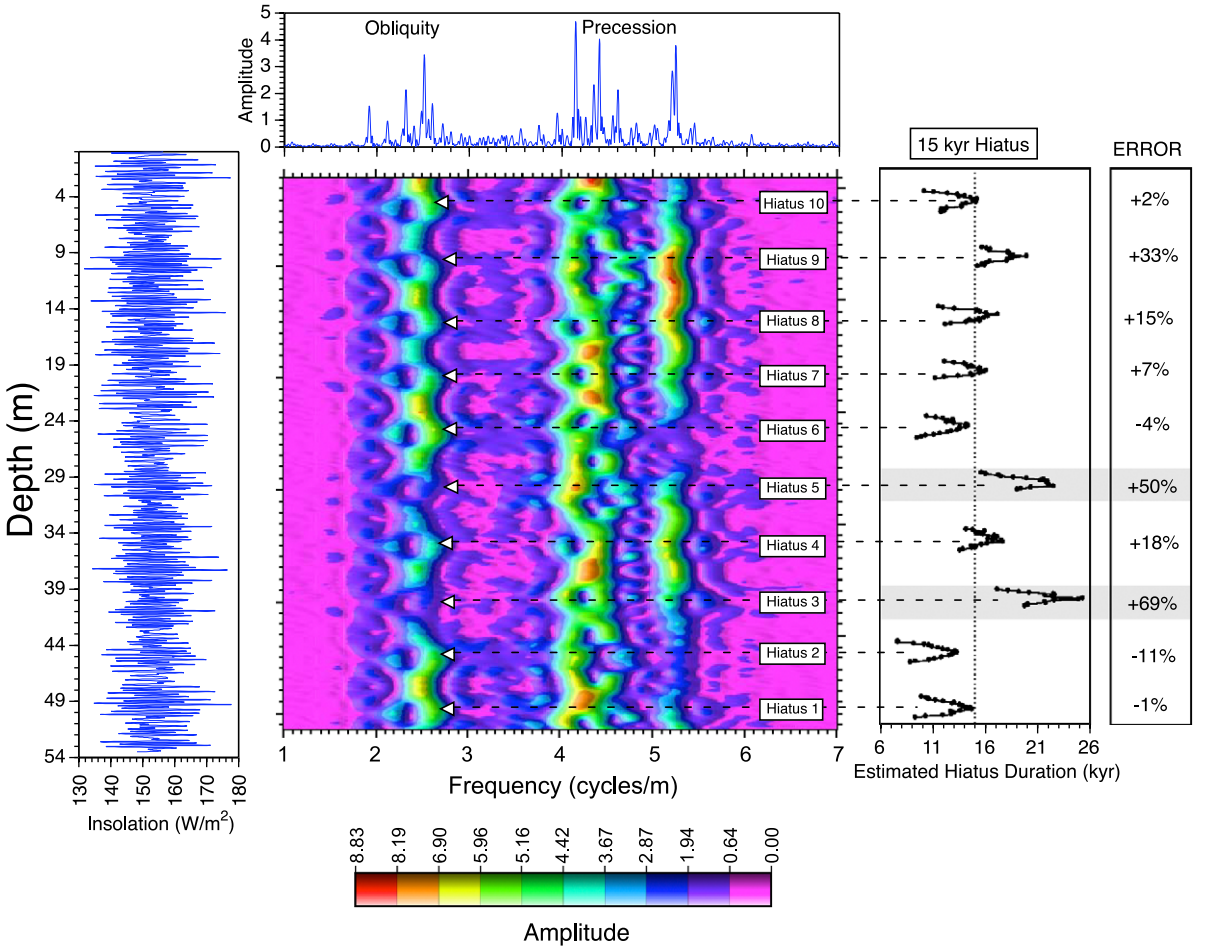

Fig. 7. EHA-$\Delta\mu$ sensitivity analysis employing the insolation data series in Fig. 6 to model 54 m of stratigraphy with 10 imbedded hiatus events of 15 kyr each (background sedimentation rate = 1 cm/kyr; sampled every 1 cm). The model data is plotted to the left of the EHA results. The amplitude spectrum for the entire data series is shown at the top of the EHA plot. The EHA analysis employed three 2π tapers and a 4-m moving window. Estimated hiatus duration and error are shown to the right of the EHA plot.

trol (e.g., based on dated bentonites) is utilized to calculate temporal periodicities from the measured spatial bedding frequencies. Second, the calculated temporal periodicity of the bifurcated component is adjusted to its closest predicted theoretical value [30]. These two approaches provide a range of potential hiatus durations.

Finally, there are several important caveats of the EHA-$\Delta\mu$ technique: (1) This method permits the identification of hiatus and quantification of its minimum duration. EHA-$\Delta\mu$ analysis of a given frequency component cannot determine if more than one wavelength of the bifurcated periodicity (P) has been removed by hiatus (e.g., for $P=40$ kyr, hiatus events of 5 and 45 kyr result in identical $\Delta\mu$ measurements). However, independent EHA-$\Delta\mu$ analysis of multiple orbital components (e.g., obliquity and long eccentricity) each of which responds differently to a hiatus of a given temporal duration, permits better constraint on the minimum possible hiatus duration. More traditional methods such as biostratigraphic zonation, radiometric dating, and geomagnetic polarity reversals may be employed to help constrain a reasonable upper limit on hiatus duration. (2) Rapid addition of sediment, such as thick volcanic ash deposits and slumping, may also generate amplitude bifurcation. Therefore, sedimentologic data from the interval of interest is important for accurate interpretation of observed amplitude bifurcations. Sediments that are deposited relatively instantaneously (such as volcanic ashes) may be removed from the data series prior to EHA-$\Delta\mu$ analysis. (3) The ability to sense and resolve relatively short hiatuses scales to frequency in that a shorter hiatus is more clearly resolvable in a higher-frequency component. Stratigraphic modeling exercises suggest that hiatus of at least 20% of a given periodicity (P) may be clearly identified throughout much of the spectrum (if $P=40$ kyr, hiatus resolution $=8$ kyr), barring severe or compound multiple distortions in sedimentation. In the lowest frequencies the ability to detect hiatus decreases slightly. However, hiatus as short as 30% of P may be identified even at the third lowest frequency in the spectrum. (4) The resolution of hiatus in low-frequency components is ultimately limited by the size of the moving window, while the resolution of hiatus in high frequency components may be limited by short-term sedimentation rate instability.

3. Application of the EHA-$\Delta\mu$ technique to the late Cenomanian Bridge Creek Limestone

3.1. Geologic background

The Bridge Creek Limestone Member (late Cenomanian–early Turonian) of the Greenhorn Limestone Formation is a rhythmic hemipelagic deposit that is primarily composed of decimeter-scale limestone/marlstone couplets that are laterally traceable for over 1000 km in the Western Interior Basin [31,32]. The unit was deposited during maximum transgression of the Greenhorn marine cycle [33,34]. The lower portion of the Bridge Creek Limestone Member contains the C/T boundary, spans Oceanic Anoxic Event II (a time of enhanced organic carbon burial worldwide), records stepwise molluscan extinction horizons [21,22], and displays a major turnover in deep-dwelling planktonic foraminifera [35].

The fine-grained hemipelagic deposits of the Bridge Creek Limestone Member include micritic to argillaceous limestones, which alternate with argillaceous to calcarenitic marlstones and shales [36]. The unit also contains bioclastic calcarenite or calcisiltite beds and lenses, which are commonly ripple laminated. Calcarenite beds (or skeletal limestones) are rare in the lower Bridge Creek Limestone Member but become common in the upper portion of the unit [36,37].

Previous workers [33,38,39] have attributed calcarenite facies in the Western Interior Basin to winnowing and/or condensation. For example, Sageman [39] interpreted skeletal limestones in the Lincoln Limestone and Hartland Shale members of the Greenhorn Formation as tempestites formed due to winnowing of bioclasts by storm wave base during sea level fall, followed by fine-grained sediment starvation during subsequent sea level rise. Although these facies clearly involve distortion of the time–rock regime well in excess of the normal variation in sedimentation rates that characterize background mudrocks, it has not been possible to rigorously quantify the temporal distortion of sedimentation associated with their formation.

The Bridge Creek Limestone Member has been a source of cyclostratigraphic interest for over a century (e.g., [1,2,37]). Sedimentary bedding cycles corresponding to Milankovitch orbital cyclicity have been

quantitatively confirmed within the unit by Sageman et al. [37,40], Meyers et al. [6], and Prokoph et al. [41]. Sageman et al. [37] documented eccentricity, obliquity, and precession cycles within the upper Bridge Creek Limestone Member (spanning the uppermost portion of the *Watinoceras devonense* biozone to the lowermost portion of the *Collignoniceras woollgari* biozone). Using multi-taper method [17] power spectral techniques, the authors identified prominent spatial frequencies in geochemical and lithologic data series based on a 5-cm sampling of the USGS no. 1 Portland core. The spatial frequencies were calibrated to temporal periodicities using two time scales developed from radiometrically dated volcanic ashes that occur within the Bridge Creek Limestone (Kauffman et al.'s [15] and Gradstein et al.'s [42] time scales, based on the $^{40}Ar-^{39}Ar$ dates of Obradovich [23]). Sageman et al.'s [37,40] analysis was restricted to the upper Bridge Creek Limestone because preliminary results from the lower portion of the unit were erratic, which the authors tentatively attributed to sedimentation rate instability and/or missing section. To refine the analysis of orbital cyclicity in the unit, particularly in the lower Bridge Creek Limestone OAE II interval, Meyers et al. [6] employed evolutive harmonic analysis to evaluate a sub-millimeter resolution optical densitometry data series from the Bridge Creek Limestone (USGS no. 1 Portland core). Calibration of the spatial bedding periods using the radiometric dates of Obradovich [23], as well as the more recent age estimates of Kowallis et al. [24], identify eccentricity, obliquity and precession in the lower Bridge Creek Limestone Member (Table 2), and confirm the previous cycle estimates of Sageman et al. [37,40]. Evaluation of the Bridge Creek EHA results in tandem with stratigraphic modeling experiments has permitted the development of a high-resolution sedimentation history for the Bridge Creek Limestone Member [6].

An alternate interpretation of the Bridge Creek orbital cyclicity has been proposed by Prokoph et al. [41] based on wavelet and spectral analysis of published wt.% OC data [19] and comparison of observed spatial frequency ratios to those predicted by orbital theory. Prokoph et al.'s [41] analysis was limited by the low and variable resolution of the wt.% OC data of Pratt et al. [19], which makes detection of higher-frequency orbital components difficult. Comparative evaluation of the orbital cyclicity within the lower

Table 2
Assessment of bedding periodicity in the Bridge Creek Limestone OAE II interval (no. 1 Portland core), identified from harmonic analysis of a 2-m optical densitometry data window centered on 2.15 m [6]

Spatial frequency (cycles/m)	Amplitude (pixel)	Frequency probability (%)	Obradovich [23] periods ($s=1.20$ cm/kyr) (kyr)	Kowallis et al. [24] periods ($s=0.99$ cm/kyr) (kyr)	After adjusting to 1.03 cycles/m to 94.78 kyr ($s=1.03$ cm/kyr)	Predicted periods (kyr)	% Difference from predicted value	Prokoph [41] estimate ($s=1.67$ cm/kyr)	Predicted periods (kyr)	% Difference from predicted value
1.03	17.31	99.89	81.02	98.38	94.78	Eccentricity = 94.78	0.00	58.33	Obliquity (O1) = 50.44	15.65
2.69	20.12	89.72	31.03	37.68	36.30	Obliquity (O2) = 38.94	− 6.78	22.34	Precession (P1) = 22.34	0.00
4.23	17.09	97.00	19.71	23.93	23.05	Precession (P1) = 22.34	3.20	14.19	?	?
5.31	11.10	93.11	15.68	19.04	18.34	Precession (P2) = 18.54	− 1.05	11.29	?	?
8.46	5.94	91.62	9.85	11.97	11.53	P1 Harmonic = 11.17	3.20	7.09	?	?

Employment of a 2-m window was required for analysis of the bedding cyclicity, due to sedimentation rate instability within the lower Bridge Creek Limestone [6]. The radiometric dates of Obradovich [23] yield a sedimentation rate of 1.20 cm/kyr, while those of Kowallis et al. [24] yield 0.99 cm/kyr. These sedimentation rate estimates suggest that the 1.03 cycle/m frequency is attributable to short eccentricity (94.78 kyr). Application of this calibration resolves the predicted precession and obliquity components with an error of $<7\%$. Calibration with the sedimentation rate estimate of Prokoph et al. [41] is shown for comparison.

Bridge Creek Limestone is provided by applying Prokoph et al.'s [41] sedimentation rate estimate (1.67 cm/kyr) to the high-resolution optical densitometry harmonic analysis results shown in Table 2, and comparison of these results to a 1.03 cm/kyr calibration. The 1.67 cm/kyr calibration resolves a potential precession component (P1), and a potential obliquity component with 15.65% error, while the 1.03 cm/kyr sedimentation rate calibration resolves four predicted orbital components (as well as the harmonic of a precession component), and accounts for all of the high-amplitude, highly significant peaks with $<7\%$ error. A more detailed comparison and evaluation of published C/T cyclostratigraphic records and OAE II chronologies (e.g., [15,41,43,44]) may be found in Meyers [45].

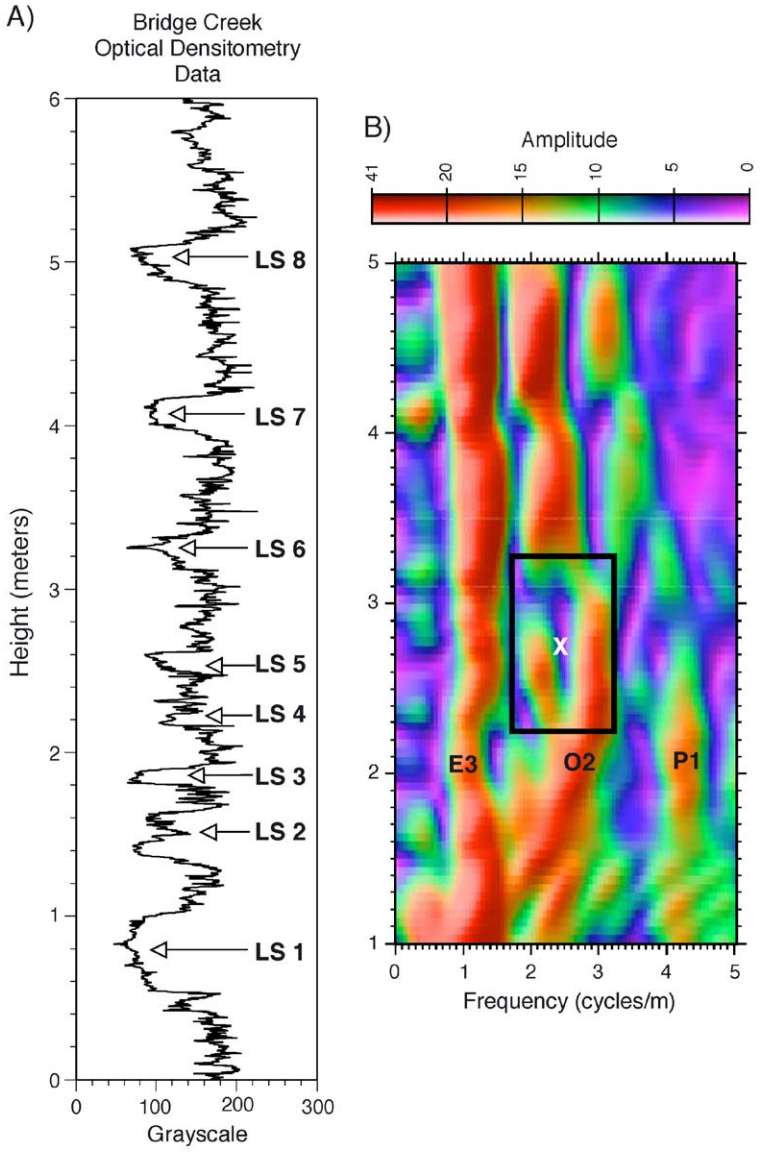

Fig. 8. EHA analysis of high-resolution optical densitometry data series (A) from the USGS no. 1 Portland core. LS1–LS8 identify the limestone marker beds of Elder [21]. The EHA time–frequency amplitude plot is shown in (B).

3.2. Lower Bridge Creek Limestone EHA-$\Delta\mu$ analysis

The high-resolution optical densitometry data series of Meyers et al. [6] (Fig. 8) was utilized for EHA-$\Delta\mu$ analysis of the lower Bridge Creek Limestone Member. Low grayscale values represent light-colored limestone, with low wt.% organic carbon content, while high grayscale values indicate dark colored marlstone, with relatively high wt.% organic carbon content and lower wt.% calcium carbonate content. This data set provides an excellent high-resolution proxy for couplet-scale compositional variability throughout the unit [6].

The time–frequency amplitude plot of this optical densitometry record is shown in Fig. 8B. The data set was investigated using a 2-m window, a 5-cm step, and $3-2\pi$ tapers. Fig. 8B displays three persistent components (~ 1, ~ 2.5, and ~ 4.5 cycles/m at ~ 2 m), which can be identified as eccentricity (95 kyr), obliquity (O2 = 36 kyr), and precession (P1 = 23 kyr) (Table 2). The gentle secular drift to lower-frequency components throughout the study interval reflects an increase in sedimentation rate up section. This plot contains a bifurcation in the 2.5 cycles/m (O2) component at ~ 2.9 m (designated by "X" in Fig. 8B). The response of $\Delta\mu$ across this bifurcated interval (2.45–3.00 m) is shown in Fig. 9C. This plot indicates a maximum $\Delta\mu$ of -0.072 at 2.65 m directly on top of limestone marker bed number 5 (LS5) of Elder [21]. Utilizing the measured obliquity periodicity of 36.30 kyr (Table 2), this yields a minimum hiatus duration of 15.8 kyr (solid line in Fig. 9D) while the predicted periodicity for obliquity of 38.94 kyr [30] yields a minimum hiatus duration of 16.9 kyr (dashed line in Fig. 9D). Note that this hiatus duration is near the detection limit for the short eccentricity component (it represents $\sim 18\%$ of 95 kyr), which is one reason that the short eccentricty signal is not distorted. The relatively small window (2 m or ~ 200 kyr) employed in the analysis prohibits identification of hiatus-related distortion in the eccentricity frequency range. Allowance for the maximum of 50% error in these estimates yields final minimum hiatus duration values of 15.8 ± 7.9 and 16.9 ± 8.45 kyr.

4. Discussion

Elder [46] observed that biozone boundaries in the C/T interval were characterized by evidence of winnowing and condensation, and suggested that they may reflect multiple diastems. However, he concluded that these disconformities are infrequent and short

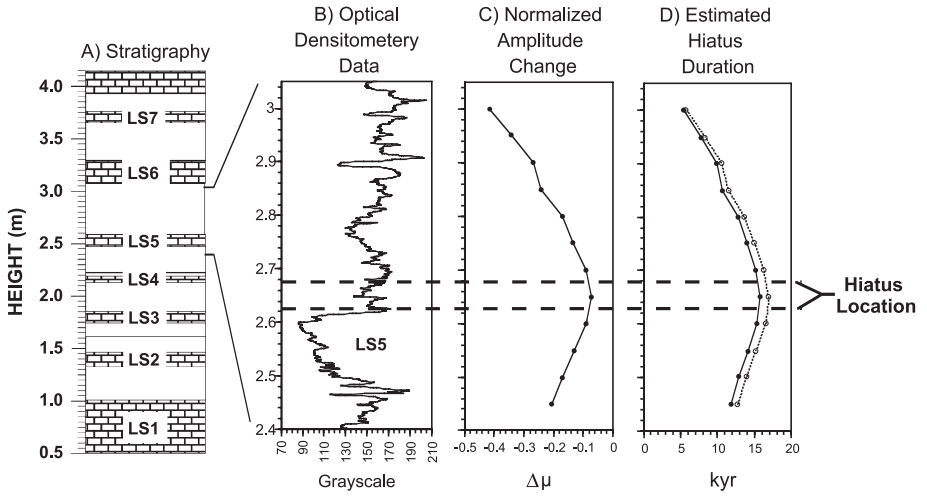

Fig. 9. $\Delta\mu$ hiatus reconstruction for the lower Bridge Creek Limestone Member. Stratigraphy (A), optical densitometry data (B), $\Delta\mu$ plot (C), and estimated minimum hiatus duration (D) are displayed for the bifurcation identified in the lower Bridge Creek Limestone Member. LS1–LS8 identify the marker limestone beds of Elder [21]. The solid line in 9D displays hiatus duration if the measured periodicity of 36.30 kyr is used. The dashed line in (D) displays the hiatus duration if the theoretical obliquity periodicity of 38.94 kyr is used.

(less than one couplet cycle) in the central basin of the Western Interior seaway. The hiatus identified by EHA-$\Delta\mu$ analysis in the USGS no. 1 Portland core (lower boundary of *Neocardioceras juddii* Biozone) at the top of LS5 is not conspicuous in core or outcrop within the central basin region. However, Elder [21] reported that the top of the LS5 limestone bed in his measured section at Rock Canyon in Pueblo, Colorado (which is near the location of the no. 1 Portland core) is conspicuously calcarenitic. It is worth noting that this is the only such calcarentic layer identified by Elder [21] in the lower portion of Bridge Creek Limestone at Pueblo (which spans the interval we have analyzed in Fig. 8). In addition, sedimentary discontinuity surfaces have been described from this stratigraphic interval in Bridge Creek Limestone sections from southwestern New Mexico [47]. They are characterized by nodular to calcarenitic limestones with evidence of erosion, reworking, and phosphatization. Disconformity at this stratigraphic level also occurs in hemipelagic deposits at other localities worldwide, such as the Plenus Marls of the Anglo-Paris Basin [48].

Basin-wide stratigraphic data sets (including bed thicknesses and biostratigraphic data) from the interval containing marker bed LS5 permit an independent test of hiatus at this stratigraphic level. Utilizing the data of Elder [46], we examine thickness trends associated with marker beds LS5, LS6, and the intervening shale (and their lateral equivalents; lithologic character of some beds changes in different parts of the basin). These beds can be recognized throughout the basin by their spatial relation to the bentonite B marker bed of Elder [21], and their biostratigraphic assemblages. Six sections were utilized to construct a west–east transect across the basin axis (Fig. 10A and B):

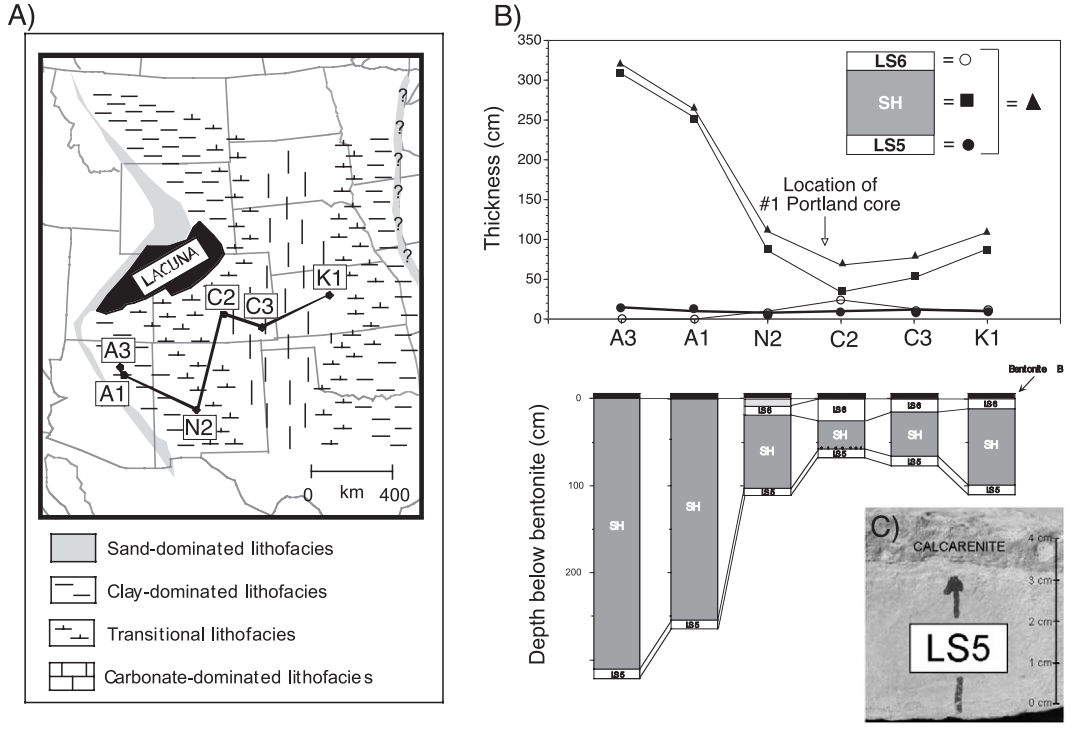

Fig. 10. (A) Lithofacies distribution in the Western Interior of the United States during deposition of the *N. juddii* biozone, with locations of the study sites (modified from Elder [50]). A1 = Blue Point, Arizona; A3 = Coal Mine West, Arizona; N2 = Carthage, New Mexico; C2 = Pueblo, Colorado; C3 = Deora, Colorado; K1 = Bunker Hill, Kansas. (B) Stratigraphic data from across the Cretaceous Western Interior Basin (data from Elder [46]). The LS5 and LS6 marker beds are displayed as white, the intervening shale as dark gray, and bentonite B as black. The light gray interval just above LS6 at Carthage, New Mexico, represents a marly shale (with 1 cm limonite bed at base) that is not present at the other localities. (C) A photo of LS5 and its calcarenitic cap (Pueblo section).

Coal Mine West (Arizona), Blue Point (Arizona), Carthage (New Mexico), Pueblo (Colorado), Deora (Colorado), and Bunker Hill (Kansas).

LS6 is thickest at the basin center (Pueblo, Colorado), decreasing in thickness to the east and west, and eventually disappearing in the west as the shoreface is approached (Fig. 10A and B). This trend is associated with an increase in the thickness of the shale bed both east and west of Pueblo. These observations are consistent with a siliciclastic/carbonate co-dilution model in which carbonate content is increasingly diluted by siliciclastic flux toward the basin margin (see lithofacies map in Fig. 10A), while the basin center is an area of relative condensation that receives considerably less siliciclastic input and preserves maximum limestone bed thicknesses. LS5 departs from the trends noted above, showing roughly equivalent thicknesses throughout the basin transect, in addition to the presence of a calcarenite cap in the basin center section (Pueblo, Colorado; Fig. 10B and C). The existence of this calcarenite cap is consistent with our interpretation of Pueblo as a region of maximum condensation and suggests that this location may be most sensitive to generation of a significant gap in sedimentation. Many other limestone marker beds in this west–east transect of the lower Bridge Creek Limestone display the same thickness trend as LS6. The limestone marker beds that deviate from this trend are generally associated with concretionary limestones, and we suggest that these bed thicknesses may have been influenced by diagenetic factors. It is notable that none of the other limestone marker beds in the lower Bridge Creek Limestone show the relatively constant bed thickness displayed by LS5.

Within the relatively condensed stratigraphic intervals at the Carthage, Deora and Bunker Hill sections, the thickness of LS5 is 1–2 cm less than LS6, but at the Pueblo location LS5 is 14 cm thinner (Fig. 10B). If the thickness trends associated with LS6 reflect the typical background siliciclastic flux/carbonate flux ratio across this transect, the stratigraphic analysis suggests that 12–14 cm of sediment is "missing" from LS5 at the Pueblo section. The EHA-derived background sedimentation rate for this interval of the Bridge Creek (0.84 cm/kyr) indicates that the absence of 12–14 cm of sediment represents 14.3–16.7 kyr of missing time. This hiatus duration estimate is consistent with the results from the EHA-$\Delta\mu$ analysis (15.8–16.9 $\pm$ 50% = 7.9–25.35 kyr) and provides an independent source of support for them. The hiatus in the stratigraphic interval of *N. juddii* becomes prominent in northwestern Colorado, eastern Utah, and southwestern Wyoming (Fig. 10A), associated with a paleobasin high [49,50].

Comparison of our results with the stepwise molluscan extinction horizons of the C/T boundary indicate that the hiatus atop LS5 is coincident with the 3rd extinction step of Elder [21,22]. This extinction horizon has the largest number of concurrent species extinctions (10), and this large number may be partially attributable to the condensation of time at this horizon. In contrast, the hiatus does not appear to have had any clear "artifactual" impact on the expression of geochemical records from the interval. However, paleobiologic and geochemical proxy records from the Bridge Creek Limestone suggest that the stratigraphic level of the hiatus marks an important sustained paleoenvironmental change within the basin. Molluscan species richness drops abruptly just above this stratigraphic horizon [21], biserial planktic foraminifera dramatically increase in abundance (the "Heterohelix shift") [51], and the rate of accumulation of organic matter increases substantially [6]. These changes have previously been hypothesized to reflect the incursion of a Tethyan oxygen minimum zone (OMZ) into the Western Interior Basin during the latter phase of the OAE II interval [6,51,52]. The coincidence of these observations with evidence for extreme condensation/hiatus worldwide (e.g., Jefferies [48]) suggests that the hiatus on top of LS5 may mark a eustatic sea level pulse that cut off detrital supply to distal locations and allowed the Tethyan OMZ to breach the southern sill of the Western Interior Basin.

We hypothesize that the hiatus identified by EHA-$\Delta\mu$ analysis reflects the confluence of siliciclastic starvation and a pronounced decline in pelagic carbonate production such that total "new" bulk sedimentation was zero for this interval. To test this hypothesis, the time scale developed by Meyers et al. [6] is employed to map spatial geochemical records from the no. 1 Portland core onto a temporal framework. These geochemical records permit assessment of changes in the flux of carbonate and detrital (terrigenous) material (the dominant sediment components) throughout the study interval. The geochemical records employed in this study represent 2-

m moving averages, which is appropriate because the time scale applied to them (to calculate accumulation rates) is based on a 2-m moving average of sedimentation rate derived from EHA. Although the time scale of Meyers et al. [6] begins at the top of marker bed LS1, in this study, we extend the time scale to the beginning of Oceanic Anoxic Event II (in the Hartland Shale Member just below LS1) by adding an additional 107 kyr. The choice of 107 kyr was based on: (1) the thickness of strata included and mean accumulation rates for the interval (calculated using radiometric data), and (2) stratigraphic evidence that LS1 separates into five distinct limestone beds in some portions of the basin (such as western South Dakota), which we interpret as a short eccentricity cycle (~ 100 kyr). See Meyers [45] and Meyers et al. [6] for a detailed description of this time scale.

Carbonate flux for the C/T interval (Fig. 11A) shows three pulses in carbonate accumulation with an occurrence interval of ~ 400 kyr. The hiatus is located in the trough at ~ 293 kyr, which suggests that it is associated with a minimum in long-eccentricity (400 kyr)-forced carbonate productivity. Analysis of the insoluble fraction (bulk sediment accumulation minus carbonate accumulation and organic carbon accumulation), which is largely composed of detrital clay with a small volcanigenic background contribution, also displays three general pulses in accumulation in the study interval (Fig. 11B). The insoluble fraction flux covaries with titanium accumulation (Fig. 11C), and these records suggest that detrital flux to the central basin may be partially forced by long eccentricity. There appears to be an overprinting of this 400-kyr Milankovitch signal by a second forcing mechanism, which results in a gradual decrease in the amplitude of the subsequent pulses of accumulation. This secular trend of decreasing detrital flux correlates with a global eustatic sea level rise to highstand [39,40,53,54], and highlights the fact that delivery of terrigenous material to the distal basin represents the interplay of Milankovitch-driven processes and other controls on terrigenious sediment delivery (e.g., subsidence controls, tectono-eustasy, etc.).

The stratigraphic horizon of the hiatus occurs within a longer-term trend of decreasing detrital flux that begins ~ 100 kyr prior to the hiatus. The 2-m moving average for insoluble residue (and titanium) accumulation rate preclude direct assessment of changes in sediment burial flux at the couplet-scale of resolution. However, the transgression–regression history of correlative shoreface deposits on the western margin of the Western Interior Basin [55]

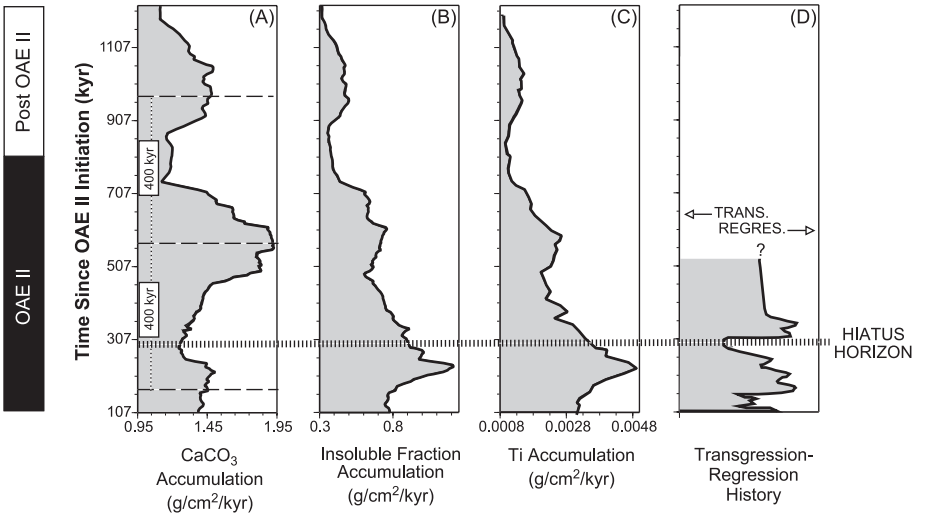

Fig. 11. (A) Carbonate, (B) insoluble fraction, and (C) titanium burial flux data from the no. 1 Portland Core. (D) Transgression–regression history from correlative shoreface deposits in Utah [55]. The hiatus is located at ~ 293 kyr.

(Fig. 11D) suggests that the hiatus occurred during an episode of pronounced transgression, which forced a transient drop in detrital flux to the central basin. We conclude that the hiatus atop LS5 reflects the confluence of a unique suite of events: a minimum in long-eccentricity-forced carbonate productivity, and a declining background detrital flux, with a superposed transgressive pulse that culminated in sediment starvation and hiatus generation. In addition to these factors, it is also possible that winnowing played an important role in the generation of the temporal gap.

5. Conclusions

In this study, a technique that permits identification and quantification of hiatus in strata that preserve periodic stratigraphic signals is presented. This technique exploits the fact that hiatus results in bifurcation of periodic components in their amplitude (μ) spectra, and that the amplitude difference between these bifurcated peaks ($\Delta\mu$) scales to hiatus duration. Modeling experiments indicate that application of the technique should be restricted to the dominant obliquity and the long eccentricity components, since short eccentricity and precession components are characterized by inherent frequency modulations (bifurcations) that may be erroneously interpreted as hiatus. These modeling experiments also indicate that a conservative estimate of error on the calculated hiatus duration is $\pm$ 50%. Such estimates provide a minimum duration for the break in deposition, and supplementary information (e.g., paleobiologic data, stratigraphic relationships within the sedimentary basin) must be employed to determine a reasonable maximum duration. Application of the method is ultimately limited to depositional settings with a narrow range of short-term (10^0–10^5 years) sedimentation rate variability, hence, it is optimal for hiatus assessment in pelagic and distal hemipelagic environments.

We employ this technique to assess stratigraphic completeness in an interval associated with rapid paleobiologic and geochemical change: the Cenomanian/Turonian boundary. Analysis of high-resolution optical densitometry data from the Bridge Creek Limestone Member (late Cenomanian–early Turonian) identifies a hiatus within the lowermost *N. juddii* biozone, with an estimated minimum duration of 15.8–16.9 kyr ($\pm$ 50% = 7.9–25.35 kyr). Stratigraphic data from throughout the basin confirms the presence of a discontinuity at this location, and background sedimentation rate estimates suggest a hiatus duration of 14.3–16.7 kyr. Comparison of the stratigraphic horizon of hiatus with geochemical data from the interval, and the transgression–regression history of correlative shoreface deposits on the western margin of the Western Interior Basin, indicates that the hiatus is associated with a minimum in carbonate productivity, a declining background detrital flux, and a pronounced short-term transgressive event.

Acknowledgements

This study was funded by the National Science Foundation (grant EAR-0001093). The authors acknowledge the contribution of samples from the USGS no. 1 Portland core by W. Dean and M. Arthur, and the USGS Core Research Center, Denver Federal Center. We also thank J. Laurin, R. Plotnick, A. Prokoph, G. Weedon, and T. Moore for insightful comments. ***[BOYLE]***

References

[1] G.K. Gilbert, Sedimentary measurement of geologic time, Geology 3 (1895) 121–127.
[2] A.G. Fischer, Gilbert-bedding rhythms and geochronology, in: E.I. Yochelson (Ed.), The Scientific Ideas of G.K. Gilbert: Geological Society of America Special Paper 183 (1980) 93–104.
[3] T.D. Herbert, S.L. D'Hondt, Precessional climate cyclicity in Late Cretaceous–Early Tertiary marine sediments: a high resolution chronometer of Cretaceous–Tertiary boundary events, Earth Planetary Science Letters 99 (1990) 263–275.
[4] M.R. House, A new approach to an absolute timescale from measurements of orbital cycles and sedimentary microrhythms, Nature 315 (1985) 721–725.
[5] J. Park, T. Herbert, Hunting for paleoclimatic periodicities in a geologic time series with an uncertain time scale, Journal of Geophysical Research 92 (1987) 14027–14040.
[6] S.R. Meyers, B.B. Sageman, L.A. Hinnov, Integrated quantitative stratigraphy of the Cenomanian–Turonian Bridge Creek Limestone Member using evolutive harmonic analysis and stratigraphic modeling, Journal of Sedimentary Research 71 (2001) 627–643.
[7] B.B. Sageman, S.R. Meyers, L.A. Hinnov, Use of orbital time

scale to evaluate molluscan biozones and evolutionary rates during the late Cenomanian–early Turonian, Western Interior Basin (USA), Eos, Trans. AGU, 2001, pp. F1140.
[8] A.B. Shaw, Time in Stratigraphy, McGraw-Hill, New York, 1964.
[9] T.C. Moore Jr., Tj.H. van Anderl, C. Sancetta, N. Pisias, Cenozoic hiatuses in pelagic sediments, Micropaleontology 24 (1978) 113–138.
[10] J. Thiede, J.W.U. Ehrmann, Late Mesozoic and Cenozoic sediment flux to the central North Atlantic Ocean, in: C.P. Summerhayes, N.J. Shackleton (Eds.), North Atlantic Palaeoceanography, Geological Society Special Publication, vol. 21, 1986, pp. 3–15.
[11] N. MacLeod, G. Keller, Hiatus distributions and mass extinctions at the Cretaceous/Tertiary boundary, Geology 19 (1991) 497–501.
[12] N. MacLeod, G. Keller, How complete are Cretaceous/Tertiary boundary sections? A chronostratigraphic estimate based on graphic correlation, GSA Bulletin 103 (1991) 1439–1457.
[13] J.L. Carney, R.W. Pierce, Graphic correlation and composite standard databases as tools for the exploration biostratigrapher, in: K.O. Mann, H.R. Lane, P.A. Scholle (Eds.), Graphic Correlation, SEPM Special Publication 53, 1995, pp. 23–43.
[14] M.R. House, The ammonoid time-scale and ammonoid evolution, in: N.J. Snelling (Ed.), The Chronology of the Geological Record, Memoir Geological Society of London 10, 1985, pp. 273–283.
[15] E.G. Kauffman, B.B. Sageman, J.I. Kirkland, W.P. Elder, P.J. Harries, T. Villamil, Molluscan biostratigraphy of the Cretaceous Western Interior Basin, North America, in: W.G.E. Caldwell, E.G. Kauffman (Eds.), Evolution of the Western Interior Basin, Geological Association of Canada Special Paper 39, 1993, pp. 397–434.
[16] G. Weedon, The detection and illustration of regular sedimentary cycles using Walsh power spectra and filtering, with examples from the Lias of Switzerland, Journal of the Geological Society London 146 (1989) 133–144.
[17] D.J. Thomson, Spectrum estimation and harmonic analysis, IEEE Proceedings 70 (1982) 1055–1096.
[18] C.J. Orth, M. Attrep Jr., L.R. Quintana, W.P. Elder, E.G. Kauffman, R. Diner, T. Villamil, Elemental abundances in the late Cenomanian extinction interval; a search for the source(s), Earth Planetary Science Letters 117 (1993) 189–204.
[19] L. Pratt, M. Arthur, W. Dean, P. Scholle, Paleoceanographic cycles and events during the late Cretaceous in the Western Interior Seaway of North America, in: W.G.E. Caldwell, E.G. Kauffman (Eds.), The Evolution of the Western Interior Basin, Geological Association of Canada Special Paper 39, 1993, pp. 333–353.
[20] S.O. Schlanger, M.A. Arthur, H.C. Jenkyns, P.A. Scholle, The Cenomanian–Turonian Oceanic Anoxic Event: I. Stratigraphy and distribution of organic carbon-rich beds and the marine $\delta^{13}C$ excursion, in: J. Brooks, A.J. Fleet (Eds.), Marine Petroleum Source Rocks, Geological Society of London Special Publication 26, 1987, pp. 371–399.
[21] W.P. Elder, Biotic patterns across the Cenomanian–Turonian extinction boundary near Pueblo, Colorado, in: L.M. Pratt, E.G. Kauffman, F.B. Zelt (Eds.), Fine-Grained Deposits and Biofacies of the Cretaceous Western Interior Seaway: Evidence of Cyclic Sedimentary Processes, SEPM, Field Trip Guidebook, vol. 4, 1985, pp. 157–169.
[22] W.P. Elder, Molluscan extinction patterns across the Cenomanian–Turonian stage boundary in the Western Interior of the United States, Paleobiology 15 (1989) 299–320.
[23] J. Obradovich, A .Cretaceous time scale, in: W.G.E. Kauffman, E.G. Kauffman (Eds.), Evolution of the Western Interior Basin, Geological Society of Canada Special Paper 39, 1993, pp. 379–396.
[24] B.J. Kowallis, E.H. Christiansen, A.L. Denio, M.J. Kunk, L.M. Heaman, Age of the Cenomanian–Turonian boundary in the Western Interior of the United States, Cretaceous Research 16 (1995) 109–129.
[25] P.B. de Menocal, Plio-Pleistocene African climate, Science 270 (1995) 53–59.
[26] J. Park, C.R. Lindberg, F.L. Vernon III, Multitaper spectral analysis of high-frequency seismograms, Journal of Geophysical Research 92 (1987) 12675–12684.
[27] J. Laskar, The chaotic motion of the solar system: a numerical estimate of the chaotic zones, Icarus 88 (1990) 266–291.
[28] D. Paillard, L. Labeyrie, P. Yiou, Macintosh program performs time series analysis, EOS, Transactions, American Geophysical Union 77 (1996) 379.
[29] A. Berger, M.F. Loutre, J.L. Melice, Instability of the astronomical periods from 1.5 Myr BP to 0.5 Myr AP, Paleoclimates 2 (1998) 239–280.
[30] A. Berger, M.F. Loutre, J. Laskar, Stability of the astronomical frequencies over the Earth's history for paleoclimate studies, Science 255 (1992) 560–566.
[31] D.E. Hattin, Widespread, synchronously deposited, burrow-mottled limestone beds in Greenhorn Limestone (Upper Cretaceous) of Kansas and central Colorado, American Association Petroleum Geologists Bulletin 55 (1971) 412–431.
[32] W.P. Elder, E.R. Gustason, B.B. Sageman, Basinwide correlation of parasequences in the Greenhorn Cyclothem, Western Interior, U.S. Geological Society of America Bulletin 106 (1994) 892–902.
[33] E.G. Kauffman, Geological and biological overview: Western Interior Cretaceous Basin, Mountain Geologist 13 (1977) 75–99.
[34] E.G. Kauffman, Paleobiogeography and evolutionary response dynamic in the Cretaceous Western Interior Seaway of North America, in: G.E.G. Westermann (Ed.), Jurassic–Cretaceous Biochronology and Paleogeography of North America, Geological Association of Canada Special Paper 27, 1984, pp. 273–306.
[35] R.M. Leckie, Foraminifera of the Cenomanian–Turonian boundary interval, Greenhorn Formation, Rock Canyon Anticline, Pueblo, Colorado, in: L.M. Pratt, E.G. Kauffman, F.B. Zelt (Eds.), Fine-Grained Deposits and Biofacies of the Cretaceous Western Interior Seaway: Evidence of Cyclic Sedimentary Processes, SEPM, Field Trip Guidebook, vol. 4, 1985, pp. 139–149.
[36] W.P. Elder, J.I. Kirkland, Stratigraphy and depositional envi-

ronments of the Bridge Creek Limestone Member of the Greenhorn Limestone at Rock Canyon Anticline near Pueblo, Colorado, in: L.M. Pratt, E.G. Kauffman, F.B. Zelt (Eds.), Fine-Grained Deposits and Biofacies of the Cretaceous Western Interior Seaway: Evidence of Cyclic Sedimentary Processes, SEPM, Field Trip Guidebook, vol. 4, 1985, pp. 122–134.

[37] B.B. Sageman, J. Rich, M.A. Arthur, G.E. Birchfield, W.E. Dean, Evidence for Milankovitch periodicities in Cenomanian–Turonian lithologic and geochemical cycles, Western Interior U.S., Journal of Sedimentary Research 67 (1997) 286–301.

[38] D.E. Hattin, Carbonate substrates of the Late Cretaceous Sea, central Great Plains and southern Rocky Mountains, Palaios 1 (1986) 347–367.

[39] B.B. Sageman, Lowstand tempestites: depositional model for Cretaceous skeletal limestones, Western Interior, U.S., Geology 24 (1996) 888–892.

[40] B. Sageman, J. Rich, C.E. Savrda, T. Bralower, M.A. Arthur, W.E. Dean, Multiple Milankovitch cycles in the Bridge Creek Limestone (Cenomanian–Turonian), Western Interior basin, in: W.E. Dean, M.A. Arthur (Eds.), Stratigraphy and Paleoenvironments of the Cretaceous Western Interior Seaway, U.S.A., SEPM, Concepts in Sedimentology and Paleontology, vol. 6, 1998, pp. 153–171.

[41] A. Prokoph, M. Villeneuve, F.P. Agterberg, V. Rachold, Geochronology and calibration of global Milankovitch cyclicity at the Cenomanian–Turonian boundary, Geology 29 (2001) 523–526.

[42] F.M. Gradstein, F.P. Agterberg, J.G. Ogg, J. Hardenbol, P. van Veen, J. Thierry, Z. Huang, A Mesozoic time scale, Journal of Geophysical Research 99 (1994) 24051–24074.

[43] L.M. Pratt, Isotopic studies of organic matter and carbonate in rocks of the Greenhorn Marine Cycle, in: L.M. Pratt, E.G. Kauffman, F.B. Zelt (Eds.), Fine-Grained Deposits and Biofacies of the Cretaceous Western Interior Seaway: Evidence of Cyclic Sedimentary Processes, SEPM, Field Trip Guidebook, vol. 4, 1985, pp. 38–48.

[44] W. Kuhnt, A. Nederbragt, L. Leine, Cyclicity of Cenomanian–Turonian organic-carbon-rich sediments in the Tarfaya Atlantic Coastal Basin (Morocco), Cretaceous Research 18 (1997) 587–601.

[45] S.R. Meyers, Integrated Cyclostratigraphy and Biogeochemistry of the Cenomanian/Turonian Boundary Interval, Western Interior Basin, North America, PhD thesis, Northwestern University, Evanston, 2003.

[46] W.P. Elder, Cenomanian–Turonian (Cretaceous) stage boundary extinctions in the Western Interior of the United States, PhD thesis, University of Colorado, Boulder, 1987.

[47] S.C. Hook, W.A. Cobban, Late Greenhorn (Mid-Cretaceous) discontinuity surfaces, southwest New Mexico, New Mexico Bureau of Mines and Mineral Resources, Circular 180 (1981) 5–21.

[48] R.P.S. Jefferies, The palaeoecology of the *Actinocamax plenus* subzone (lowest Turonian) in the Anglo-Paris Basin, Paleontology 4 (1961) 609–647.

[49] E.A. Merewether, W.A. Cobban, Biostratigraphic units and tectonism in the mid-Cretaceous foreland of Wyoming, Colorado, and adjoining areas, in: J.A. Peterson (Ed.), Paleotectonics and Sedimentation in the Rocky Mountain Region, United States, AAPG Memoir, vol. 41, 1986, pp. 443–468.

[50] W.P. Elder, Molluscan paleoecology and sedimentation patterns of the Cenomanian–Turonian extinction interval in the southern Colorado Plateau region, in: J.D. Nations, J.G. Eaton (Eds.), Stratigraphy, Depositional Environments, and Sedimentary Tectonics of the Western Margin, Cretaceous Western Interior Seaway, GSA Special Paper 260, 1991, pp. 113–137.

[51] R.M. Leckie, R.F. Yuretich, O.O. West, D. Finkelstein, M. Schmidt, Paleoceanography of the southwestern Western Interior sea during the time of the Cenomanian–Turonian boundary (late Cretaceous), in: W.E. Dean, M.A. Arthur (Eds.), Stratigraphy and Paleoenvironments of the Cretaceous Western Interior Seaway, U.S.A, SEPM, Concepts in Sedimentology and Paleontology, vol. 6, 1998, pp. 101–126.

[52] M.A. Arthur, B.B. Sageman, W.E. Dean, R.L. Slingerland, L.R. Kump, T.S. White, Transgression, advection of oxygen-depleted water, and eutrophication of the mid-Cretaceous Western Interior Seaway of North America, Geological Society of America Annual Meeting Abstracts with Program, 1998, p. 396.

[53] E.G. Kauffman, Cretaceous evolution of the Western Interior Basin of the United States, in: L.M. Pratt, E.G. Kauffman, F.B. Zelt (Eds.), Fine-Grained Deposits and Biofacies of the Cretaceous Western Interior Seaway: Evidence of Cyclic Sedimentary Processes, SEPM, Field Trip Guidebook, vol. 4, 1985, pp. IV–XIII.

[54] B. Haq, J. Hardenbol, P.R. Vail, Chronology of fluctuating sea-level since the Triassic, Science 235 (1987) 1156–1167.

[55] J. Laurin, Effects of relative sea level fluctuations and other controls in linked nearshore and hemipelagic depositional settings; examples from the Bohemian Cretaceous Basin and the U.S. Western Interior, PhD thesis, Charles University, Prague, 2003.